Polymer Degradation and Stability 223 (2024) 110743

Contents lists available at ScienceDirect

Polymer Degradation and Stability

journal homepage: www.journals.elsevier.com/polymer-degradation-and-stability

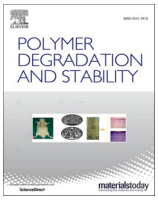

Optimal processing conditions of a bio-based epoxy synthesized from vanillyl alcohol

S. Zaidi [b], S. Thakur [c], D. Sanchez-Rodriguez [b,*], R. Verdejo [c], J. Farjas [b], J. Costa [a]

[a] AMADE - Analysis and Advanced Materials for Structural Design, Polytechnic School, University of Girona, C/ Universitat de Girona 4, E-17003 Girona, Spain
[b] GRMT Materials Research Group and Thermodynamics, Polytechnic School, University of Girona, C/ Universitat de Girona 4, E-17003 Girona, Spain
[c] Polymer Composite Group, Institute of Polymer Science & Technology ICTP, CSIC, C/Juan de la Cierva 3, E-28006 Madrid, Spain

ARTICLE INFO

Keywords:
Processability map
Thermoset
Bio-based
Epoxy resins
Vanillin
Thermal oxidation

ABSTRACT

This work provides a comprehensive thermomechanical and rheological characterization of a high-performance epoxy resin synthesized from a vanillin derivative, vanillyl alcohol. The study includes a complete analysis of the curing and decomposition kinetics that enabled a Time-Temperature-Transformation plot accounting for gelation, vitrification, and resin degradation to be developed. These plots allow one to determine the optimal time and temperature processing conditions that will yield the best mechanical properties. Kinetic predictions and experimental results showed that this resin can be cured at room temperature in just a few hours, forming a solid gelled glass. Enhanced mechanical properties are achieved by post-curing the resin at temperatures above $T_{g\infty}$ = 85.4 °C. With a dynamic storage modulus of 2.7 GPa, this bio-based resin proves to be a sustainable alternative to fossil-based resins whose primary source is the ever-prevalent bisphenol A diglycidyl ether. Thermal oxidation is the main cause of the mechanical deterioration at high temperatures, as revealed by FTIR spectroscopy.

1. Introduction

Thermosetting epoxy resins are known to have excellent mechanical properties along with thermal and corrosion resistance. In addition, they offer good adhesion to a broad variety of surfaces and are readily available on the market. These characteristics have made them the preferred choice for multiple industrial applications [1] such as matrices for fiber-reinforced materials [2,3], structural adhesives [4,5], paints [6,7] or high-performance coatings [8,9]. The extensive use of epoxy resins has an inherent environmental cost arising from their thermosetting nature; the stability of these cross-linked polymers makes recycling extremely challenging, if not impossible. On top of that, most epoxy resins are derived from petroleum-based compounds, including bisphenol A which is the source of 90 % of all commercially available resins [10]. Scientists have struggled to find alternative synthesis methods that make use of renewable feedstock and lessen environmental impacts. Nevertheless, this pursuit for an alternative eco-friendly substitute to traditional thermoplastic counterparts has led to so-called bioplastics. On the other hand, the development of bio-based thermosets is not as advanced given that they have received comparatively less attention [10], although epoxy resins have been successfully produced from the epoxidation of vegetable oils [11,12] or from aromatic-containing biomass sources [13,14]. Besides, their thermo-mechanical characteristics typically do not match those of commercial fossil-based epoxy networks [15], making the search for high-performance bio-based thermosets a major issue.

Lignin is the most abundant natural aromatic compound on Earth [16] and because of this some of the most valuable chemicals for bio-based epoxy resins are lignin derivatives. Among them, vanillin, (the main component of natural vanilla), deserves special mention as it is one of the few aromatic compounds that can be synthesized from wood on an industrial scale [17]. Advances in vanillin production from lignin depolymerization have dispelled some of the initial environmental concerns [18] that had arisen from their synthesis, making it a sustainable and low-cost process [17] and placing it ahead of other bio-based chemicals that rely on much less developed technologies. Besides, vanillin is also obtained as a byproduct of the biomass refinery [19]. Vanillin-based epoxy resins have been shown to have comparable mechanical properties to those prepared from the well-known bisphenol A diglycidyl ether epoxide DGEBA. For example, Desnoes et al. prepared a cured thermoset epoxy made from diglycidyl ether Schiff base monomers from vanillin which has proved to be a suitable alternative to DGEBA-based epoxy in high-performance coatings [20]. Recently, Zhi et al. successfully developed a sustainable vanillin-based epoxy resin

* Corresponding author.
E-mail address: daniel.sanchez@udg.edu (D. Sanchez-Rodriguez).

https://doi.org/10.1016/j.polymdegradstab.2024.110743
Received 1 December 2023; Received in revised form 7 March 2024; Accepted 11 March 2024
Available online 12 March 2024

with good flame retardancy and with even higher storage modulus and glass transition temperature (Tg) than DGEBA. Both were cured using the same 4,4′-diaminodiphenylmethane hardener [21]. Furthermore, Savonnet et al. presented a novel approach using divanillin-based epoxy precursors that led to bio-based thermosets with phase transitions and thermal stabilities comparable to the DGEBA-based network. Therefore, vanillin-based epoxies are clearly promising substitutes to bisphenol A for designing high-performance thermosets for structural composite and adhesive applications [15]. In this paper, we present a new synthesis method of a bio-based epoxy resin from vanillyl alcohol as the primary resource with promising thermal and mechanical properties. Our study includes a characterization of the structure of the epoxy network by Fourier-Transform Infrared Spectroscopy (FTIR), and an evaluation of its thermomechanical characteristics determined by dynamic mechanical analysis (DMA).

Resin processability is as important to its market uptake as to its performance. For this reason, a meaningful evaluation of the resin must also include a thorough study of the curing process. Time-Temperature-Transformation (TTT) diagrams are particularly useful for optimizing resin curing cycles and have been previously applied to epoxy thermosets for such purposes [22–25]. Recently, we extended the classical TTT curing diagram to include thermal stability, thus leading to a more complete and useful processing chart [26]. Such a chart allows us to identify the optimal conditions under which we can achieve complete cure while avoiding degradation. This diagram relies on predictions obtained from kinetic studies. The simplicity of this tool compared to complex simulations facilitates rapid decision making at the processing stage, ultimately contributing to the adoption of high-performance bio-based thermoset and advancing towards the uptake of sustainable material solutions. With the aim of generating the corresponding processability map, the curing and decomposition kinetics of our vanillin-based resin were investigated via thermal analysis methods. Additionally, thermally induced chemical changes were monitored by FTIR.

2. Experimental section

2.1. Materials

Vanillyl alcohol (4-hydroxy-3-methoxybenzyl alcohol, 99 %), epichlorohydrin, sodium hydroxide (97 %), tetrabutylammonium bromide (99 %, phase transfer agent and catalyst), and anhydrous magnesium sulfate were purchased from Sigma-Aldrich (Germany). A commercial curing agent (sd4772) was obtained from Sicomin, France, and supplied by Mel Composites (Barcelona, Spain). Solvent, ethyl acetate was purchased from Scharlau.

2.2. Synthesis of bio-based epoxy resin from vanillyl alcohol

The bio-based epoxy was synthesized from vanillyl alcohol as the bio-based resource. A round-bottom flask with a reflux condenser was charged with vanillyl alcohol, epichlorohydrin and phase transfer catalyst, and heated to 100 °C for 5 h with continuous stirring. Next, using an ice bath, the flask was cooled to ~0 °C before adding a 40 wt% NaOH solution dropwise and then allowed to slowly warm to room temperature over the course of 1 h. After that, the reaction mixture was dissolved in ethyl acetate, washed thrice with DI water, dried over anhydrous magnesium sulfate, and concentrated under reduced pressure. The successful synthesis of the bio-epoxy monomer was confirmed by means of FTIR analysis (Figure S1): the FTIR spectrum shows a prominent absorption band at 913 cm^{-1} corresponding to the presence of the oxirane ring. The peaks identified at 1182 and 1508 cm^{-1} are attributed to the stretching vibrations of aromatic C–O and aromatic C=C bonds, respectively. The distinctive peaks appearing at 1200–1250 cm^{-1} signify the presence of phenol C–O groups. The characteristic absorption band around 2869 cm^{-1} confirms the existence of the methoxy structure ($-OCH_3$) in vanillyl alcohol derivatives. Notably, the FTIR spectrum provides confirmation that the initial epoxy resin lacked any oligomeric byproduct, as evidenced by the absence of the OH group.

For the curing process, the resulting epoxy monomer was mixed with a commercial curing agent (SD4772 from Sicomin) at a ratio of 30 phr (parts of hardener per 100 parts of resin). This proportion was determined to be approximately the stoichiometric ratio of the mixture, such that it was the epoxy-to-hardener weight ratio yielding a maximum heat of reaction (ΔH) [27,28] (Fig. 1). Hence, ΔH at maximum, 460.4 J/g, corresponds to the enthalpy of reaction. This value is within the normal enthalpy range of epoxy-amine systems [27,29,30].

2.3. Calorimetric measurements

The curing reaction was monitored using a differential scanning calorimeter (DSC) Q2000 from TA Instruments. For that purpose, experiments were conducted at various heating rates ranging from 1.25 to 20 °C/min within a temperature range of 0 to 260 °C. Uncured samples were placed in Tzero low mass aluminum crucibles and tested in an inert atmosphere, maintained by a nitrogen gas flow rate of 50 mL/min. An empty Tzero low mass pan was used as reference. Based on an analytical criterion [31] intended to prevent inaccuracies when determining the sample temperature in thermal analysis experiments, we have used samples masses bellow 10 mg in all the tests. The curing kinetic parameters, including the apparent activation energy of the reaction and pre-exponential factor, were calculated using the Friedman isoconversional method outlined in Section (2.8). The evolution of the glass transition temperature, Tg, with the degree of cure was also characterized by means of DSC tests. To do so, various uncured samples were heated up to different temperatures at a speed of 10 °C/min, targeting different maximum temperatures as summarized in table S1. The corresponding DSC scans are depicted in Figure S2. In compliance with the standard methodology, Tg was determined from the midpoint of the extrapolated onset and endset transition temperatures. The degree of cure was predicted from the recorded evolution of the sample temperature during the test, which includes the cooling step.

2.4. Fourier-transform infrared spectroscopy

Fourier-Transform Infrared Spectroscopy (FTIR) was used to study the structural changes associated with the thermal degradation of the resin. Infrared spectra of samples were collected with an ALPHA

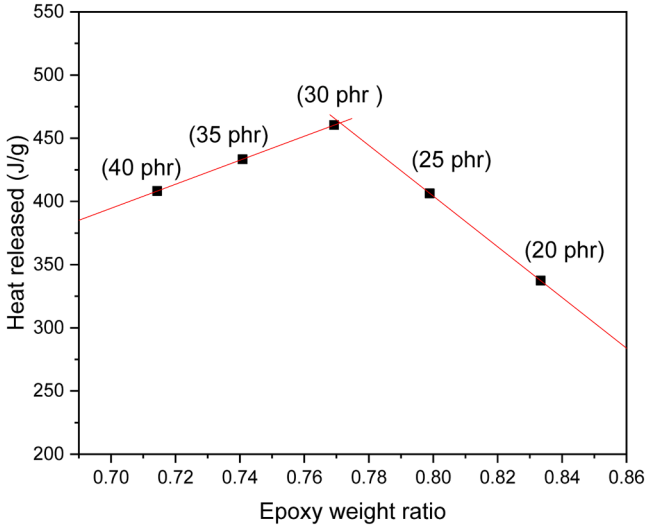

Fig. 1. (single column fitting image) Dependence of heat released with the epoxy-to-hardener weight ratio. In brackets, the corresponding parts of hardener per 100 parts of epoxy for the measured points.

spectrometer from Bruker, in attenuated total reflection (ATR, model Platinum). A sample was heated at 20 °C/min, and then rapidly quenched upon reaching the target temperature. Afterwards, the sample was analyzed and then heated again to a higher target temperature. Targeted temperatures were in the range of 100 to 300 °C at intervals of 50 °C. The IR spectra were obtained after averaging 24 consecutive scans over a wavenumber range between 500 and 4000 cm^{-1} in transmission mode. The spectra interpretation was based on the practical approach proposed by Coates [32].

2.5. Thermogravimetric study

A Mettler Toledo thermobalance (model TGA/DSC1), was used to monitor the thermal degradation of the cured resin by thermogravimetry (TG). A series of measurements were carried out at different heating rates, from 1.25 °C/min to 20 °C/min, under a gas flow of 60 mL/min of synthetic air, using samples of approximately 6 mg and Al_2O_3 crucibles of 150 μL volume. In addition, simultaneous TGA/FTIR measurements were performed to identify the main volatile gases evolved during decomposition. To that end, the outlet of the TGA furnace was connected to an ALPHA Bruker FTIR through a 40 cm long steel tube that was heated to 200 °C to prevent condensation.

2.6. Rheological study

The evolution of the viscoelastic properties of the resin during the curing process was characterized using an Anton Paar rheometer MCR 302e. The uncured sample was subjected to a rotation oscillation test employing a parallel plate geometry, with a constant shear strain of 5 % at a frequency of 1 Hz. The gap (distance between plates) was consistently maintained at 1 mm. Isothermal measurements were conducted at four different temperatures ranging from 50 to 100 °C.

2.7. Dynamic mechanical analysis

Mechanical testing of 80 × 10 × 2 mm^3 specimens cured under different conditions was carried out using a Mettler Toledo DMA SDTA861 by single frequency deformation in three-point bending. Samples were analyzed at a frequency of 1 Hz. Experiments were conducted under constant heating from 20 to 200 °C at a rate of 2 °C/min. Besides this, the T_g of the samples was determined from the thermograms as the temperature at the maximum intensity of the loss modulus peak [53].

2.8. Kinetic predictions

This work follows the same methodology as in [26] to predict the evolution of solid state transformations. The approach consists, first, in using an isoconversional method [33–37] to determine the dependence of the kinetic parameters on the degree of transformation, α, i.e., the apparent activation energy, E_α, and the pre-exponential factor, $A_\alpha f(\alpha)$. In particular, we have used Friedman's method [35]. Then, the kinetic evolution is directly determined from the time integration of the transformation rate, $d\alpha/dt$, according to the method of Farjas and Roura [38,39]:

$$\alpha_{k+1} = \alpha_k + A_\alpha f(\alpha_k) exp\left(-\frac{E_{\alpha k}}{RT_k}\right)\Delta t \tag{1}$$

Here, $E_{\alpha k}$ and $A_\alpha f(\alpha_k)$ are discrete values of E_α and $A_\alpha f(\alpha)$ for a given degree of transformation α_k. Discretization is based on constant time intervals, Δt, so that $t_k = k\ \Delta t$. Where, k is a natural number, and the thermal history is discretized as $T_k = T(t_k)$.

It is important to note that these kinetic predictions are only reliable if no significant temperature gradients are generated during processing. This is a critical issue in resin curing as the exothermic reaction can trigger a thermal runaway in samples surpassing a critical thickness, where heat dissipation fails to compensate heat generation [40,41]. In previous works we experimentally and numerically investigated the formation of thermal gradients under isothermal conditions [26,42] and we applied such knowledge to the processing of laminates considering factors such as heat generation, propagation, and boundary conditions involving thermal convection and mold contact [26]. This resulted in an analytical expression that sets the critical thickness for a thermal runaway to occur during curing, w_c, as a function of temperature.

$$w_c = w_o\left[2-\left(1+0.63\left[h\frac{w_0}{k}\right]^{1.2}\right)^{-1}\right]\left[1+1.6\frac{c}{q}\Delta T_{max}-1.1\left(\frac{c}{q}\Delta T_{max}\right)^2+2.3\left(\frac{c}{q}\Delta T_{max}\right)^3\right], \tag{2}$$

where,

$$w_{c,0} = \sqrt{\delta_{c,0}\frac{k}{\rho q}\frac{RT_m^2}{A\ E_a}e^{E_a/RT_m}}, \tag{3}$$

$$\delta_{c,0} = 2e^{-\theta_{Max}}\ \mathrm{arcosh}^2\left(e^{\theta_{Max}/2}\right), \tag{4}$$

$$\theta_{Max} = E_a\frac{\Delta T_{Max}}{RT_m^2},\ \text{and} \tag{5}$$

$$\Delta T_{Max} = 1.18684\frac{RT_m^2}{E_a}. \tag{6}$$

and c is the specific heat capacity, q is the enthalpy of the reaction, k is the thermal conductivity, ρ is the density, T_m is the mold temperature, A is the pre-exponential factor, E_a is the activation energy and h is the effective convective coefficient.

In this work, we have used these same relationships to set the critical thickness above which the thermal stability of the resin is not guaranteed due to overheating. At the same time, we are establishing a criterion to identify when our isothermal predictions might lack reliability. For the context of hot plate processing, where one side of the laminate is exposed to the atmosphere, we estimate the effective convective coefficient, h, to be approximately 70 $W/(m^2K)$ [43,44]. On the other hand, under the hot press processing, we assume a perfect thermal contact in both sides of the plate. Thus, h is infinite. As for the thermal conductivity we have used a value of 0.2 $W{\cdot}m^{-1}{\cdot}K^{-1}$, typical for epoxies. For parameters A and Ea we used a representative value taken from the kinetic study.

3. Results and discussion

3.1. Curing

Fig. 2a. shows the DSC thermograms obtained from the dynamic curing of the bio-based epoxy-hardener system upon constant heating at

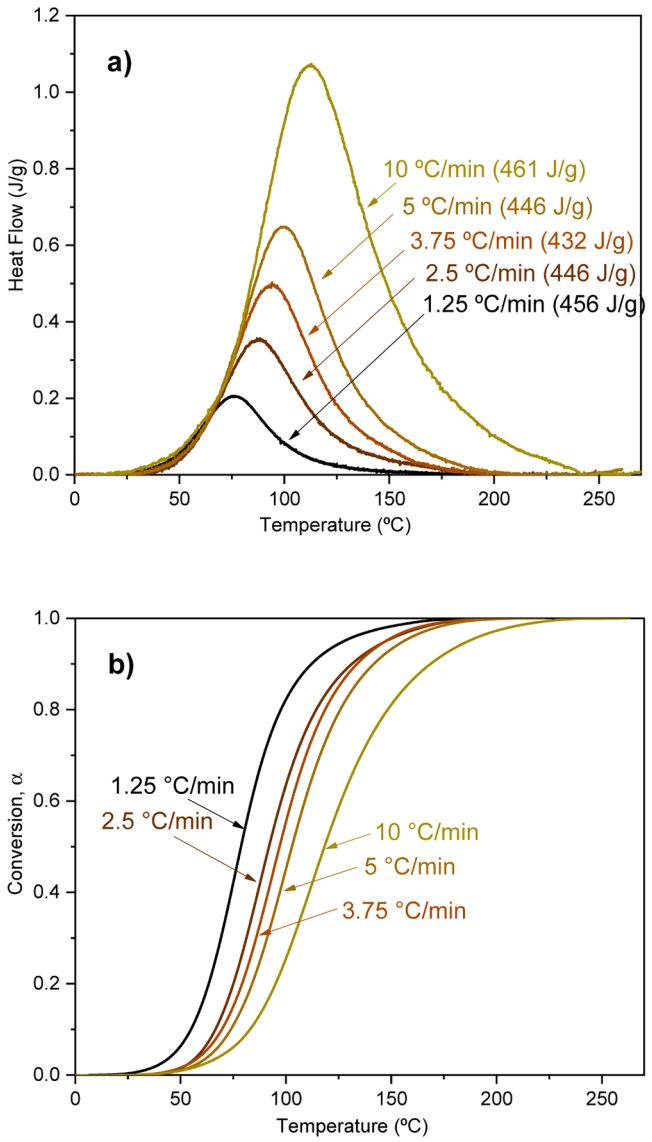

Fig. 2. (2-column fitting image) a) DSC thermograms of the bio-based epoxy system when curing at different heating rates. b) Corresponding degree of cure as a function of temperature obtained from the integration of DSC thermograms.

various rates. All the experiments reveal a unique exothermic reaction peak, which is assigned to the cross-linking reaction. The graph includes the heat of the cure determined from the area under the DSC signal. The overall heat released during the curing process is close to 450 J/g for all experiments. This value agrees comparatively with the experiments conducted to determine the stoichiometric epoxy-hardener ratio (Fig. 1). Discrepancies between different measurements may derive from the difficulty in establishing a good baseline. The corresponding conversion lines (Fig. 2b) show that, even for the slowest heating rates, all curves undergo a smooth evolution. Thus, we can neglect any perturbation on the kinetics caused by the non-isothermal vitrification of the resin [45]. The dependence of the apparent activation energy, E_α, on the degree of cure results from the Friedman's isoconversional analysis using the conversion curves is depicted in Fig. 3. The apparent activation energy remains constant within the 55 to 65 kJ/mol range, until conversion rates reach 80 %, which is in agreement with published data for epoxy-amine systems [23,25,26]. From this degree of cure onwards, there is a sustained raise in the energy required for the reaction to proceed, a trend widely reported and diversely justified, including

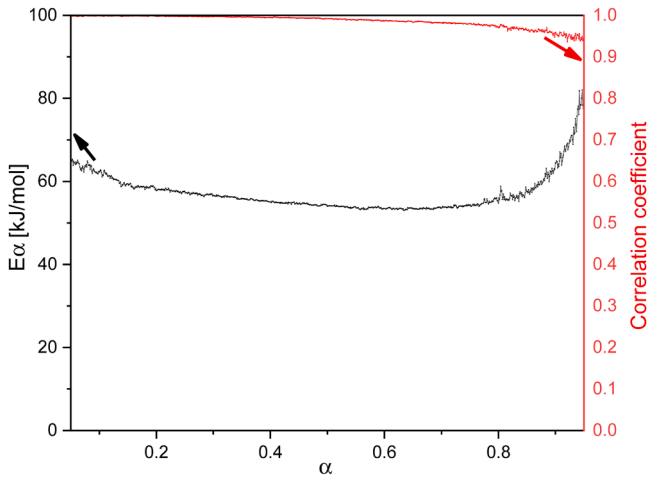

Fig. 3. (single column fitting image) Dependence of the apparent activation energy, E_α, on the degree of curing, α.

diffusion-related limitations [26,46–48] or the steric hindrance of secondary amines [26,49]. In any case, in this work we approach this issue from a purely phenomenological point of view with the sole purpose of providing valid predictions. With this in mind, the high correlation coefficient obtained in the isoconversional fit (Fig. 3) ensures the robustness of the method and its ability to predict the curing degree for a temperature range that covers most practical situations.

Fig. 4 shows the viscoelastic behavior of the hardener-epoxy system during curing under isothermal conditions at four different temperatures. All tests indicate that initially the mixture behaves as a liquid since the shear loss modulus, G'', is several orders of magnitude greater than the shear storage modulus, G'. As the sample cures, both moduli increase rapidly. However, G' increases at a much higher rate than G'' up to the point where the elastic component predominates, thus consolidating the transition from liquid to solid. In rheology measurements, the gel point can be approximately taken as the temperature where G' equals G'' [50]. Based on these experimental measurements, α_{gel}, can be then determined from the kinetic analysis. Table 1 summarizes the predictions of α_{gel} for each isothermal measurement. It is noteworthy that the predicted values of α_{gel} remain fairly constant, ranging between 0.37 and 0.4. These results confirm the isoconversional nature of α_{gel}, (i.e., for a given thermoset it corresponds to a constant degree of cure), irrespectively of the temperature history [51]. Gelation in epoxy-amine systems typically occurs between 50 and 60 % conversion [52]. Lower α_{gel} is commonly attributed to the high functionality of the building blocks [53].

We have characterized gelation kinetics by fitting the data of Table 1 to an Arrhenius temperature dependence model:

$$\ln t_{gel}(T) = A - E_{gel}/RT. \tag{7}$$

Fig. 5 shows the logarithmic representation of the gel time as a function of the reciprocal of the curing temperature in Kelvins. From the linear regression slope, we obtain an activation energy of 57.6 kJ/mol, a result that agrees closely with the apparent activation energies obtained from the isoconversional analysis shown in Fig. 3; E_α =55.4 kJ/mol at the gel point (α=α_{gel}).

We have also established the relationship between the glass transition temperature and the degree of cure to predict vitrification using the Di-Benedetto-equation [54,55]:

$$\frac{(T_g - T_{g0})}{(T_{g\infty} - T_{g0})} = \frac{\lambda\alpha}{(1-(1-\lambda)\alpha)} \tag{8}$$

where, $T_{g\infty}$ and T_{g0} are the glass transition temperatures of the fully cured resin and that of the initial mixture of monomers (zero degree of

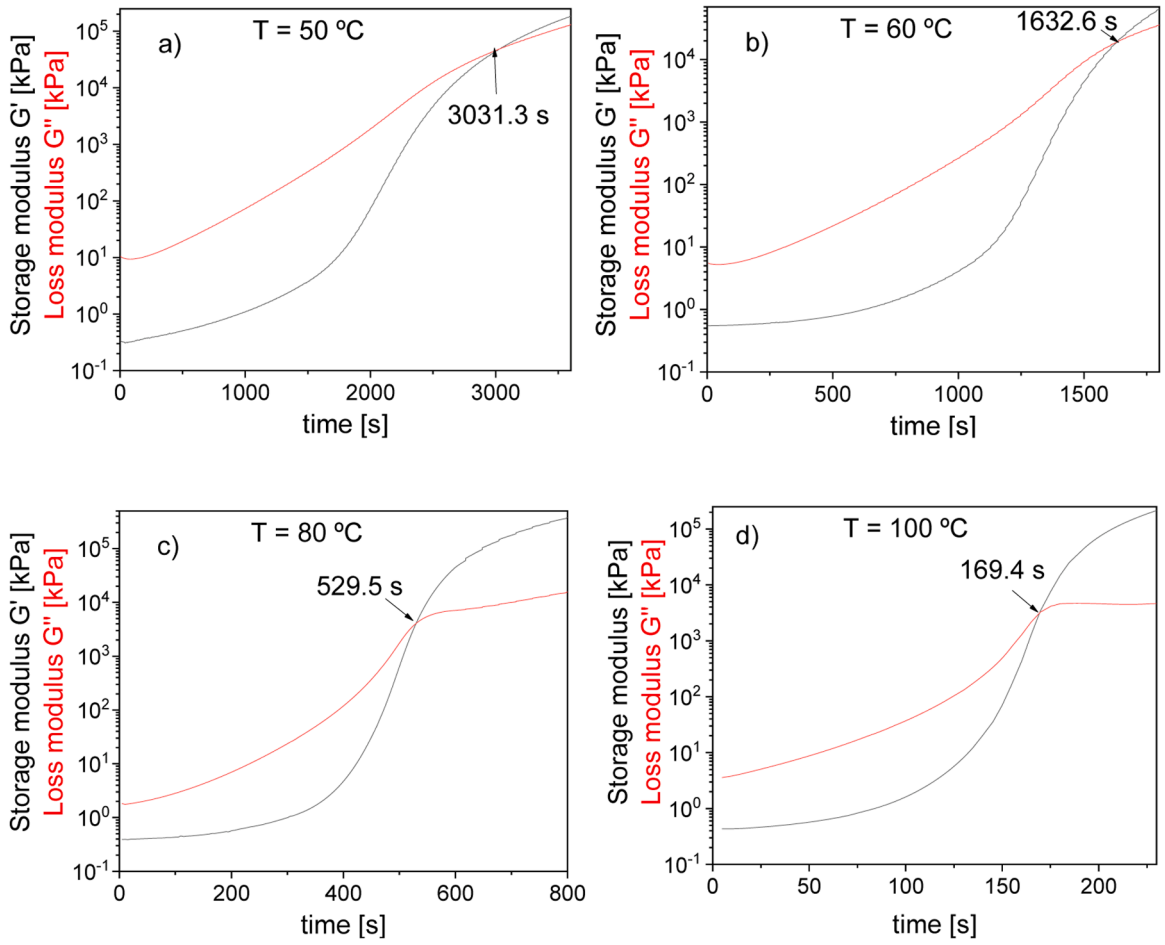

Fig. 4. (2-column fitting image) Isothermal rheological time sweep experiments of the bio-based epoxy resin.

Table 1
Gelation time at different temperatures and the corresponding degree of conversion determined from kinetic predictions.

Temperature (°C)	t_{gel} [s]	α_{gel}
50	**9289.6**	**0.37**
60	**3659.4**	**0.38**
80	**2357.7**	**0.40**
100	**1479.9**	**0.39**

cure), respectively. The parameter λ lies between 0 and 1 and can be understood as the ratio of the isobaric heat capacities of the fully reacted and uncured resin [55]. This work takes λ as a fitting parameter.

Fig. 6 shows the evolution of the glass transition temperature as curing progresses. The T_g smoothly devolves from an initial T_{g0}= −45.4 °C to a $T_{g\infty}$ = 85.4 °C at the completion of the reaction. Experimental points fit Eq. (2) with a lambda of 0.571±0.026 (R^2=0.996). To put this in perspective, the $T_{g\infty}$ of this bio-based resin is similar or even higher than that of some commercial DGEBA adhesives used for mechanical repairs of damaged components such as the ARC 858 from A.W. Chesterton ($T_{g\infty}$ = 69.5 °C) and the Steel Ceramic ($T_{g\infty}$ = 89 °C), produced by MultiMetall [52]. It is higher also than the DGEBA-TETA system ($T_{g\infty}$ = 71 °C) [56] with multiple applications as a binding and coating material in the aerospace, marine and infrastructure sectors [57].

Note that the α-T_g relationship depicted in Fig. 6 can alternatively be viewed as the α_{max}-T_{proc} relation, where T_{proc} is the processing temperature, indicating the point where curing transitions from being reaction-controlled to diffusion-limited. Therefore, α_{max} represents the maximum degree of curing above which our predictions become

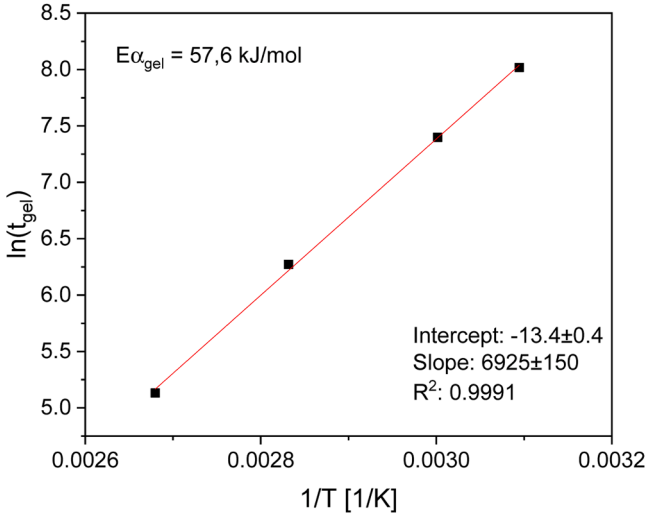

Fig. 5. (single column fitting image) Logarithm of the gel time plotted against the reciprocal of the processing temperature.

unreliable at such particular T_{proc}. In this study, we have chosen not to characterize the kinetics beyond α_{max}, as once the sample vitrifies, the predictions lose relevance from a processing perspective due to a significant decrease in the reaction rate.

We have experimentally validated the reliability of the model under isothermal conditions. To this end, we have treated several samples

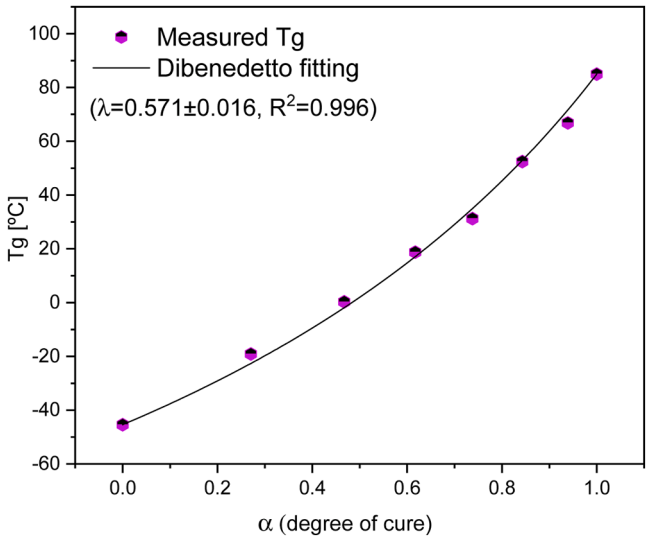

Fig. 6. (single column fitting image) Evolution of the glass transition temperature, T_g, with the degree of cure.

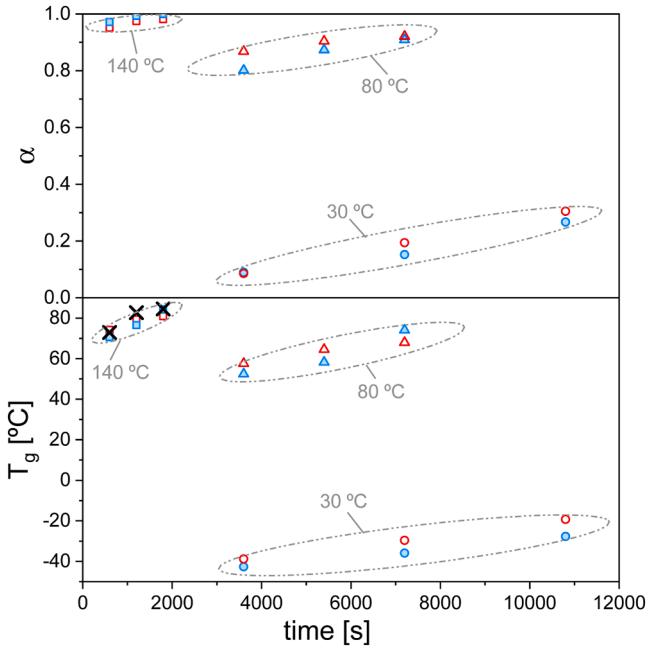

Fig. 7. (1.5-column fitting image) Experimental validation of the isoconversional model for predicting curing kinetics under isothermal conditions at different temperatures (circles: 30 °C; triangles: 80 °C; squares: 140 °C). Comparison between predicted values (empty red marks) and experimental measurements (filled blue marks) for the degree of conversion (above) and the glass transition temperature (below). X marks show measured T_g values for samples that underwent an initial curing step at low temperature (see Section 3.3).

placed in hermetic aluminum pans in a silicon bath, maintaining various constant temperatures and durations. DSC scans of these treated samples are provided in Figures S3, S4, and S5. In Fig. 7, we present a detailed comparison between the predicted degrees of cure and those measured by calorimetry, derived from the residual enthalpy of reaction. Additionally, we have compared the measured glass transition temperature (T_g) with predictions generated using the Dibenedetto fitting method, which also relies on isoconversional predictions. The findings from Fig. 7 confirm that the model effectively predicts kinetics with fair

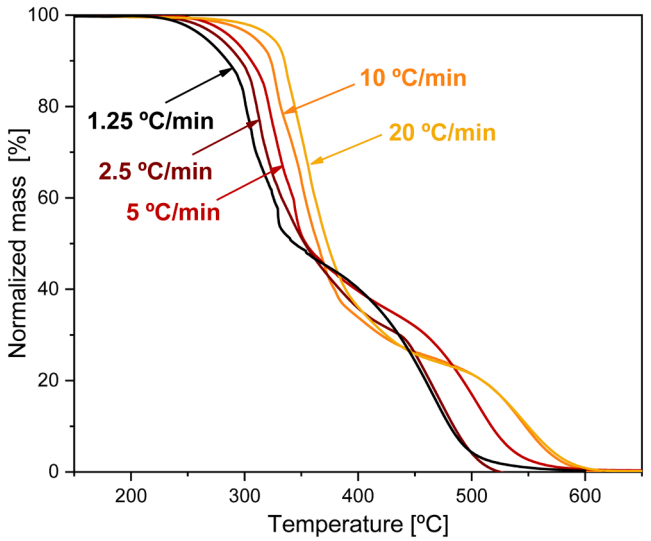

Fig. 8. (single column fitting image) TG thermograms of the cured resin heated at different heating rates.

accuracy across the 30 to 140 °C temperature range for both short and long durations, encompassing most practical situations. This validation is accomplished either by directly confirming degree of curing through residual enthalpy or indirectly through T_g measurements.

3.2. Degradation

The mass evolution when the fully-cured sample is heated in air at different heating rates decreases steadily above an onset temperature (Fig. 8). The degree of thermal decomposition relates directly to this mass loss. All thermograms exhibit two main mass loss steps: an initial process entailing irreversible structural changes, followed by the complete combustion of the resin. Only the initial stage of the first process is relevant in practical terms. When combustion becomes relevant, degradation would be so significant as to rend the polymer useless. In particular, it is important to characterize the onset of degradation as this determines the maximum temperature of service.

FTIR spectroscopy upon heating revealed the structural changes that could cause mechanical deterioration. Fig. 9 illustrates the main molecular alterations induced in the range from 1550 to 1850 cm^{-1}, where

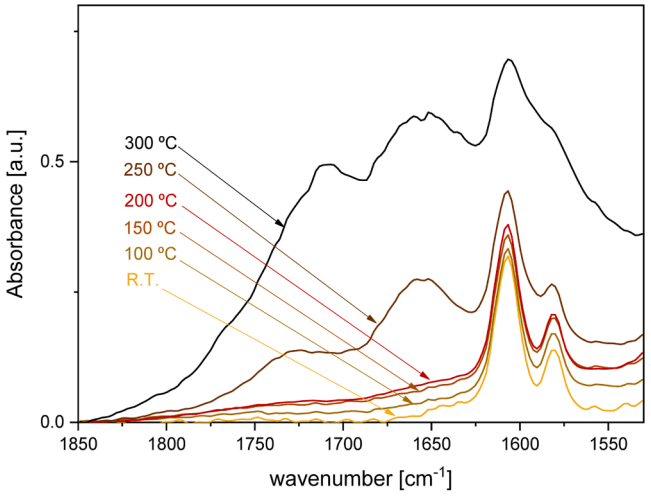

Fig. 9. (single column fitting image) FTIR spectra of the cured resin heated up to different temperatures according to the procedure described in Section 2.4.

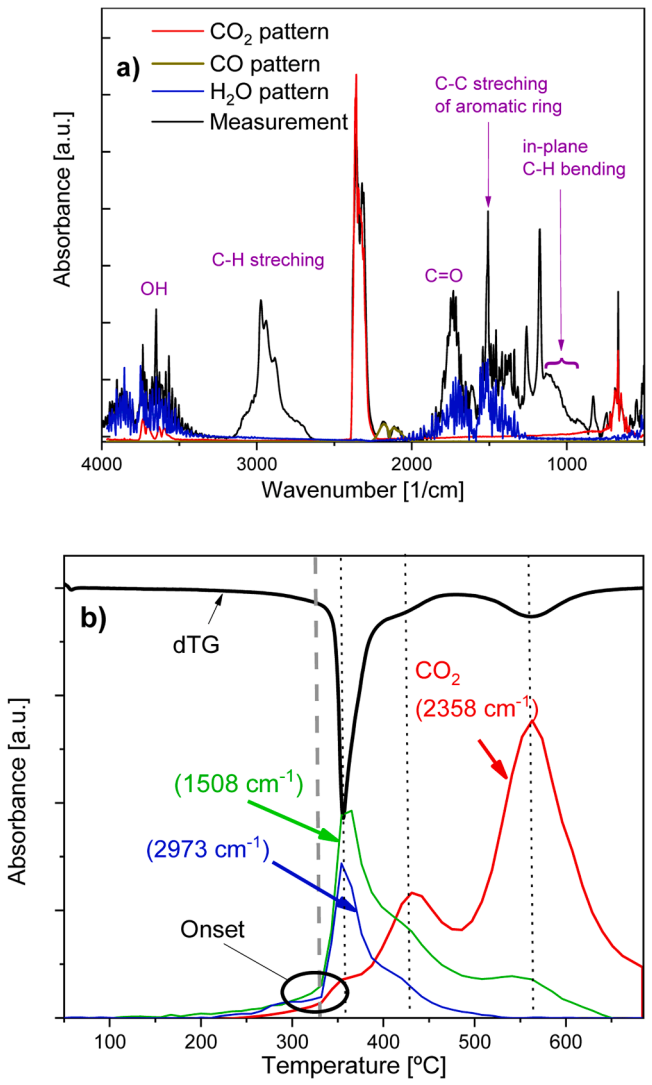

Fig. 10. (single column fitting image) a) FTIR spectrum of volatiles detected during the thermal oxidation of the resin. Spectrum registered at 356 °C for a sample heated at 20 °C/min b) TG-FTIR of the cured resin heated at 20 K/min.

structural changes associated with thermal oxidation manifest [58]. Up to 200 °C, no structural changes occur. All spectra show two well-defined peaks at 1580 and 1610 cm^{-1}, which are attributed to the bending of amino groups and the C=C stretching of aromatic rings, respectively [59]. The first indications of degradation appear above 200 °C with the growth of two new bands at 1650 and 1730 cm^{-1}. These peaks correspond to the formation of amide and carbonyl groups, the most distinctive sign of thermal oxidation in epoxy resins [58,60].

Thermal oxidation appears with an appreciable mass loss observed in the TG curves (Fig. 8), suggesting a degradation mechanism involving chain scissions. Fig. 10.**a** shows a characteristic IR spectrum of the volatiles evolving at 356 °C from a sample heated at 20 °C /min, right at the peak of the dTG signal (Fig. 10.**b**). It reveals the release of gases such as CO_2, CO and H_2O vapor, while the remaining peaks are consistent with the simultaneous generation of several organic species such as aliphatic hydrocarbons and organic compounds: the peaks found in the 3200 to 2700 cm^{-1} region are characteristic of hydrogen-carbon-containing molecules and are assigned to several C—H stretching modes [32]; the multiple band structure in the 1150–950 cm^{-1} region along the intense peak at approximately 1510 cm^{-1} correspond to the in-plane C—H vibrations and C—C stretching of aromatic compounds, respectively [32,59]. Likewise, the sharp peak around 3600 cm^{-1} is consistent with the emission of phenolic compounds [32,61]. When plotting the evolution of some of these characteristic peaks (Fig. 10.**b**), one notices that they do coincide with the mass loss rate determined from the dTG signal. While at low temperatures the decomposition is dominated by the emission of organic volatiles, curves of 1508 and 2973 cm^{-1} wavelengths, whereas at high temperatures the emission of carbon dioxide (combustion) dominates. The evolution of the organic volatiles is not progressive. After an initial pseudo-induction period at a slow rate mass loss, (reaching 5 % mass loss), there is a sudden rate increase associated to thermal oxidation becoming critical. We take this point as the onset for thermal degradation.

Analogously to the curing analysis, we used Friedman's method to evaluate the degradation kinetic parameters from the dynamic TG experiments of Fig. 8. For the analysis, we defined 100 % degradation conversion as the physical state achieved when the mass is virtually zero [26,62]. The dependence of the apparent activation energy, E_α, on the degree of decomposition when thermal oxidation prevails over combustion reveals a gradual increase from 80 kJ/mol up to roughly 200 kJ/mol (Fig. 11). The high correlation coefficient of the isoconversional fitting ensures the reliability of the predictions. In the following, we will use this adjustment to establish an overcuring criterion.

We validated the decomposition kinetic model with a TG experiment designed to closely emulate isothermal testing conditions. The procedure involves an initial stabilization stage at room temperature, followed by a heating ramp at maximum furnace power up to the degradation temperature, an isothermal stage at the degradation temperature, and a subsequent cooling ramp down to room temperature. Another stabilization stage at room temperature concludes the process. These initial and final stabilization stages enable the thermobalance to accurately measure the initial mass and monitor the mass throughout the cooling stage. The experimental evolution of the degree of conversion has been compared to the predicted evolution, taking the sample temperature evolution recorded by the apparatus as input (Fig. 12). The results demonstrate that the kinetic model successfully predicts the kinetics of degradation across the range of degradation degree of interest allowing us to accurately predict the above defined onset for thermal degradation.

3.3. Processing map

Following our previous work [26], we propose a TTT chart to assist in choosing the appropriate processing conditions of this bio-based resin (Fig. 13.**a**). Such a diagram relies on the curing and decomposition kinetic analyses of Sections 3.1 and 3.2, respectively, and accounts for

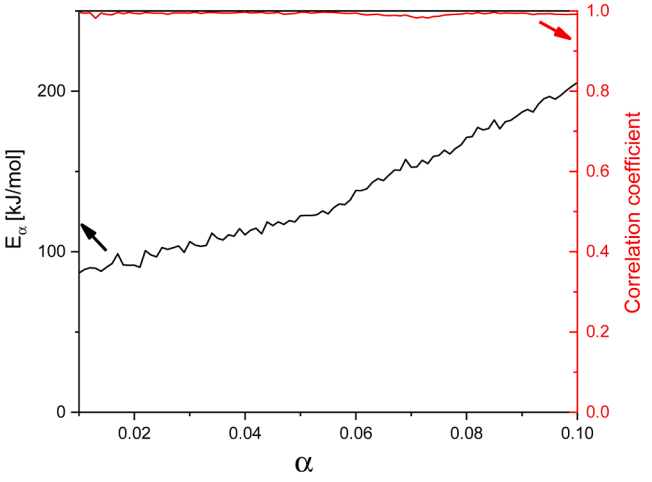

Fig. 11. (single column fitting image) Dependence of the apparent activation energy, E_α, on the degree of conversion, α, for the thermal degradation of the resin.

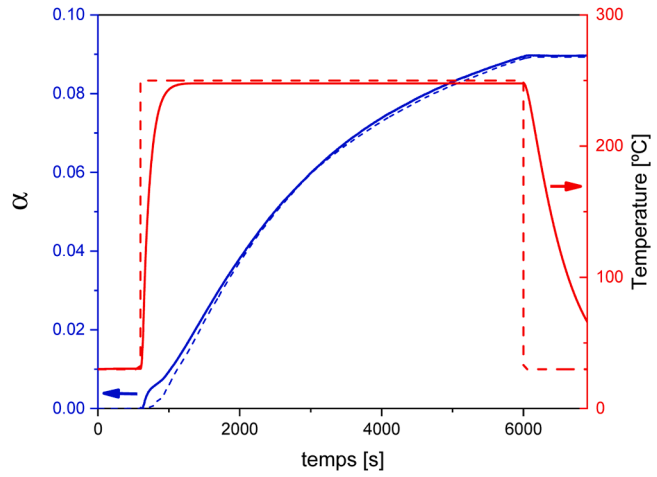

Fig. 12. (single column fitting image) Experimental validation of the iso-conversional model for predicting degradation kinetics under isothermal conditions. The left axes depict the comparison between the predicted degree of conversion (dashed blue line) and experimental measurement (solid blue line). On the right axes, the programmed thermal history (dashed red line) is contrasted with the measured evolution of the sample temperature (solid red line).

undesirable side effects such as thermal degradation or vitrification.

Fig. 13.**a** shows, in blue, several predicted isothermal conversion-time lines spanning from a degree of cure of 50 % to 99 %. The diagram indicates the glass transition temperature corresponding to each degree of conversion. Predictions extend over the 10 to 250 °C temperature range, where the required curing times span 5 orders of magnitude. In addition, we have added the gelation transition characterized in Fig. 5. Likewise, based on the evolution of Tg with the degree of cure, we have predicted the time to vitrification under isothermal conditions. The vitrification line delimits the region where the sample has reached the glassy state. Note that, even at a temperature as low as 10 °C, the resin gels before it vitrifies, i.e., it forms a gelled glass [63]. This is not a trivial observation, as the difference between forming gelled ($T_{cure}>T_{g,gel}$) or ungelled glass ($T_{cure}<T_{g,gel}$) entails that the sample would maintain its consistency during a potential post-curing process in the first case, but not in the second. Besides the low temperature, the relatively short time it takes to obtain a solid part with little or no heating is also remarkable. For example, the predictions indicate that it is possible to cure this bio-based resin at 30 °C in just a few hours. Precisely, the gelation point is exceeded after just 2.5 h of treatment, and vitrification is achieved in slightly less than 10 h. We have experimentally confirmed this through experimental observations. Fig. 14 exhibits the different frames of the time evolution of a sample that has been kept at 30 °C. After 2 h (Fig. 14.a), the resin remains in the liquid state with a honey-like viscosity. Three hour later, (i.e., after 5 h), the gelation condition has been met: continuous covalently bonded chains were extending throughout the macroscopic sample as the entire mixture became a single semi-rigid solid (Fig. 14.b). Finally, after keeping the sample at 30 °C for a whole day, it became completely rigid (Fig. 14.c). The observed progression of the rheological properties is in full agreement with our diagram (Conditions labeled as A, B and C in Fig. 13), thus validating its low temperature region.

The vitreous state is a metastable phase in which the reaction becomes diffusion controlled [64]. As the reaction slowly progresses toward equilibrium, internal stresses associated with molecular conformation changes may occur [65]. As a result, some macroscopic properties of the material might evolve over time (e.g. brittleness), which can greatly impair the mechanical performance of the polymer [66]. This phenomenon, known as physical aging, can be characterized by calorimetry through the enthalpy of relaxation that the resin undergoes when heated above its glass transition [67,68]. Fig. 15 shows a DSC scan of the sample cured at 30 °C after having spent 2 days at room temperature. The signal shows an intense endothermic peak revealing that the resin has been aging at room temperature (solid line in Fig. 15). In the transition from the glassy to the rubbery state, the sample relaxes stresses in an irreversible endothermic process that is not observed in a second scan performed immediately after the first one (dashed line in Fig. 15). In this second scan, the characteristic heat-capacity jump of the glass transition can be clearly seen. Note that the curing has progressed to a T_g higher than 50 °C, significantly above the 30 °C at which the sample vitrified.

Curing the sample at low temperatures impairs performance. Superior mechanical properties require post-curing the resin at temperatures above $T_{g\infty}$. However, thermal degradation may no longer be negligible at too high temperatures and treating the resin for an unnecessarily prolonged period might severely hinder its mechanical response. We

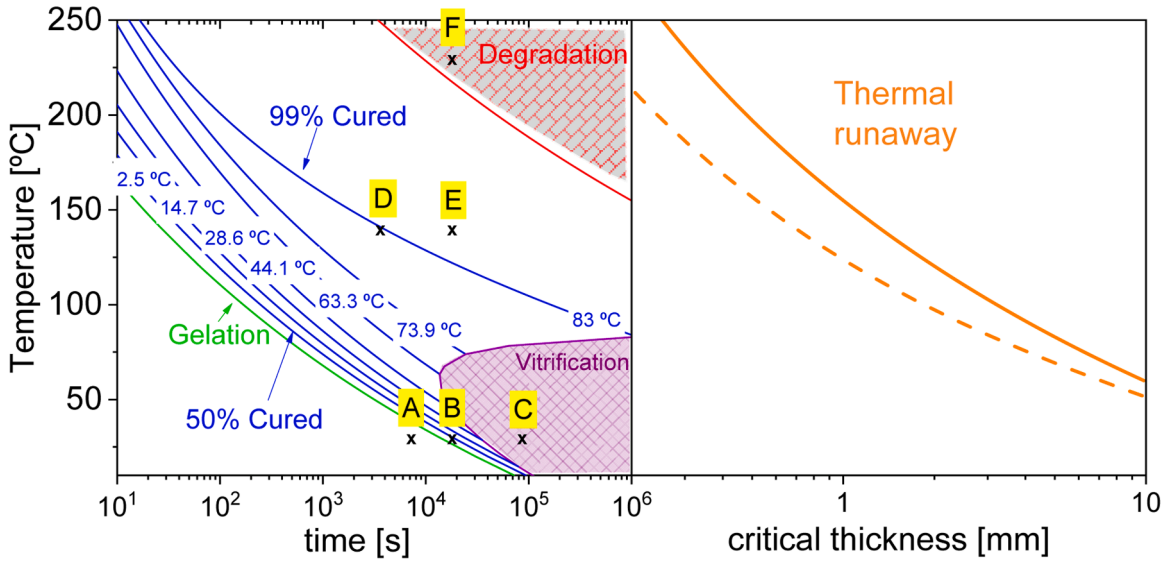

Fig. 13. (color should be used in print; **2-column fitting image**) Processing map: a) Blue lines show the time required to reach a certain degree of cure leading to a given glass transition temperature under isothermal conditions. Red line sets the onset for thermal oxidation based on the criterion stablished in Section 3.2. Green dashed line and the purple solid line indicate the time required for gelation and verification, respectively. b) critical threshold at which the sample is expected to experience a thermal runaway (solid line: hot press); solid line: convection heat losses are considered (hot plate).

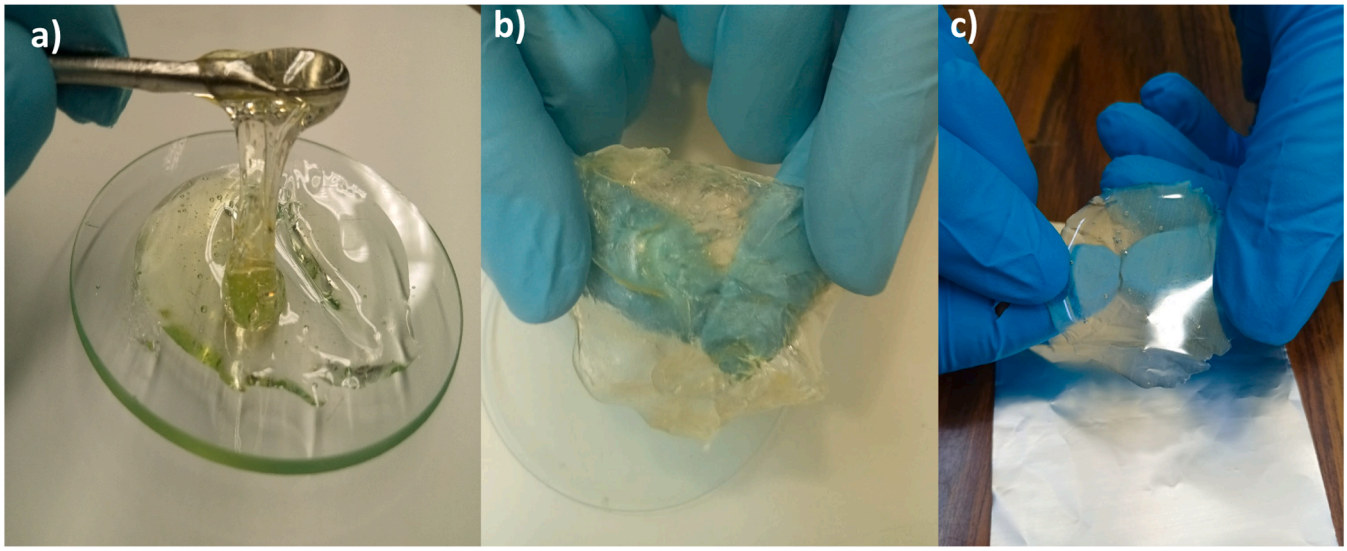

Fig. 14. (2-column fitting image) Different time frames showing the evolution of the rheological properties of the bio-based resin during the curing at 30 °C: (a) 2 h, b) 5 h and c) 24 h.

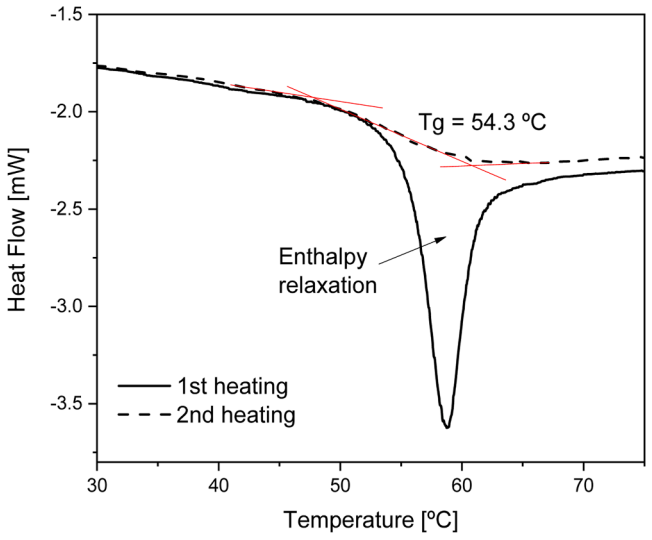

Fig. 15. (single column fitting image) DSC scan at 10 °C /min of sample cured at 30° for 2 days (solid line) showing the characteristic enthalpy relaxation profile of a physically aged thermosetting polymer. Dashed line shows a subsequent DSC scan of the same sample in which the irreversible endothermic peak is not observed.

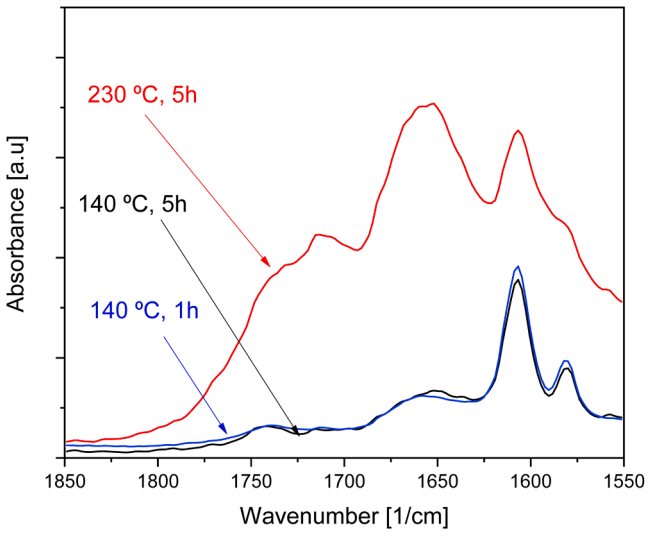

Fig. 16. (single column fitting image) FTIR spectra of the post-cured resin held at different temperatures during different timeframes.

have included the onset for thermal degradation under isothermal conditions in the processing chart. The delimited area defines the region where the sample has been overcured, revealing that the resin will experience considerable degradation within a few hours at temperatures higher than 250 °C, yet maintains thermal stability for weeks when temperatures remain below 150 °C. The optimal post-curing conditions should aim to achieve a high degree of crosslinking while avoiding entering into the thermal degradation zone. Note that the TTT diagram is still useful to roughly estimate the post-curing conditions, as the low degree of transformation achieved in the first stage of processing accounts for only a small fraction of the total post-processing time at higher temperatures. To illustrate this point, we replicated the series of isothermal experiments at 140 °C that we used to validate the kinetic model, but this time including a first stage curing at 30 °C for 5 h (Fig. 7). The DSC scans of the post-cured samples are detailed in Figure S6. The results demonstrate that, in practical terms, the impact of the initial low-temperature stage on the prediction of T_g is not significant.

As stated above, over-curing results from prolonged exposure to excessive temperatures. To exemplify overcuring experimentally, we have post-cured 3 samples that were initially processed at 30 °C up to vitrification, under different conditions (Conditions D, E and F in Fig. 13). The corresponding IR spectra of the post-cured specimens are shown in Fig. 16. Sample D (Fig. 13) was post-cured at 140 °C for 1 h, and expected to reach a degree of cure of approximately 99 %. The very low intensity of the IR peaks associated with thermal oxidation indicate that the specimen has suffered little or negligible degradation. Moreover, sample E does not show any evidence of degradation either, despite extending the post-curing time at 140 °C up to 5 h. Likewise, the amide and carbonyl bands do not grow either; in accordance with the predictions. In contrast, sample F, treated for 5 h at 230 °C, shows an IR spectrum reflecting a very intense thermal oxidation, validating the degradation criterion.

Degradation of the resin involves a change in color (Fig. 17). The samples treated for 5 h at 140 °C show the same colorless, almost transparent, appearance of the epoxy monomer, while the sample

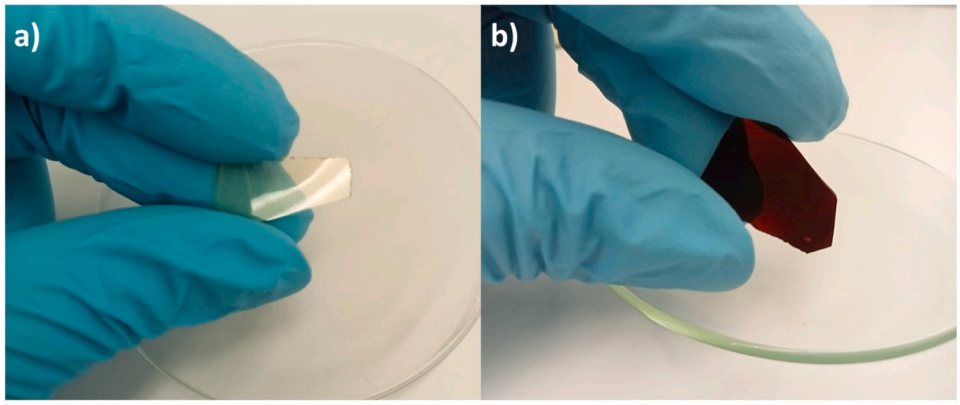

Fig. 17. (color should be used in print; **1.5-column fitting image**) a) Sample post-cured at 140 °C for 5 h; b) sample post-cured at 230 °C for 5 h.

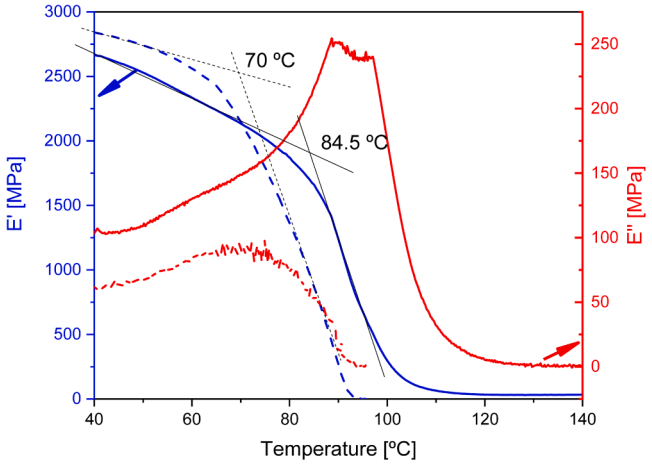

Fig. 18. (single column fitting image) DMA thermograms showing the evolution of the tensile storage and loss moduli as a function of temperature obtained from two samples processed in accordance with conditions E (solid lines) and F (dashed lines). Test were performed in air at a constant heating rate of 2 °C /min.

treated at 230 °C has darkened, turning brownish (Fig. 17).

Fig. 18 illustrates the dynamic mechanical analysis thermogram of two specimens processed following the conditions E and F. The thermogram reveals a single mechanical relaxation over the temperature range from 40 to 140 °C, which is attributed to the glass transition region. Such broad glass transition region can be associated with a high damping capacity [31]. For the sample treated at 140 °C we obtained a T_g of 84.5 °C which corresponds to the extrapolated onset of the storage modulus reduction [69]. This criterion roughly provides an upper temperature threshold for practical applications of the resin. Furthermore, it aligns well with the $T_{g\infty}$ obtained from DSC measurements for the fully-cured resin, pointing to the predicted high degree of cure (> 99 %, Fig. 11). In the sample treated at 230 °C, the effect of chain scission manifests itself through a decrease in T_g down to 70 °C. The detrimental impact of degradation is further highlighted by looking at the temperature at which the maximum intensity of the loss modulus peak occurs. This criterion, although less commonly employed in the literature, provides another valid method for determining T_g. For samples E and F, this method yields values of 88 °C and 75 °C, respectively.

Concerning the tensile storage modulus, E', at room temperature we obtained 2.7 GPa and 2.85 GPa for the low and high temperature post-cured samples, respectively. This dynamic property relates to the stiffness of the polymer [31]. The storage modulus of this bio-based resin is comparable to that of other vanillin-based structural epoxies with thermomechanical properties similar to DGEBA. For example, high performance polymers based on divaniline epoxides synthesized in [18] gave an E' within 2.12 to 3.49 GPa and were comparable to the 3.12 of the DGEBA polymer they used as a reference.

From this analysis, it is evident that overcuring significantly influences thermo-mechanical properties. Although it is beyond the scope of this work, correlating the evolution of modulus and other mechanical properties, such as impact resistance, with the degree of degradation would enhance the predictive value of processing diagrams based on TTT-plots.

Overcuring for prolonged periods of time is not the only reason that can negatively affect the mechanical properties of the resin. Ensuring a uniform temperature distribution during resin processing is key to avoid undesirable effects such as non-uniform curing, matrix degradation or even delamination [70–72]. Besides, the absence of significant thermal gradients within the sample it is necessary to accurately rely on kinetic predictions. Of particular concern is the risk of thermal runaway, especially in thick samples, were heat generation can exceed heat dissipation [40,41]. Using the analytical criteria outlined in Eq. (2), Fig. 13.b illustrates the critical thickness at which curing progresses into a thermal runaway. The dashed line corresponds to conditions applicable to hot press processing, while the solid line represents those for hot plate processing. Within the temperature range of 50 to 250 °C, this critical thickness exponentially decreases 3 orders of magnitude from approximately a centimeter to a tenth of a millimeter. This result underscores the limitations of relying solely on TTT diagrams without taking geometric factors into account. The synergistic use of both Figs. 13.a and 13.b presents a more robust methodology for effectively determining the most suitable processing conditions.

4. Conclusions

A novel bio-based epoxy thermoset was successfully prepared from a vanillin-based epoxy and commercial amine-based hardener from Sicomin showing promising thermos-mechanical properties. Curing and degradation kinetics of the resin have been characterized, thus allowing the construction of a TTT diagram to assist with defining optimal processing conditions. The diagram reveals a wide processing window for this resin within the parameter range of existing commercial epoxy resins [73], greatly facilitating its introduction into the market. The diagram takes into account vitrification, gelation, and thermal degradation, and has been experimentally validated. The processing diagram and its experimental validation confirm the following findings:

- E_α obtained using Friedman's isoconversional method ranges between 55 and 65 kJ/mol for a conversion of less than 80 %, in line with the typical behavior observed in epoxy-amine systems. This characterization does not describe reaction kinetics in the glassy

state. However, it effectively identifies the vitrification transition. The resin can cure at temperatures as low as room temperature, gelling at an α_{gel} = 38.5 % prior to vitrification. However, low temperature curing causes physical aging to occur at room temperature which embrittles the polymer. This, together with the resulting low T_g, underlines the importance of post-curing.

- An optimal post-curing allows thermomechanical properties to be attained that are similar to those obtained with commercial resins based on DGEBA. In particular, the resin can reach an elastic modulus of 2.7 GPa and a T_g of 85 °C.
- Analysis of thermal degradation kinetics is characterized by an E_α that gradually rises from 80 kJ/mol to roughly 200 kJ/mol in the initial stages of decomposition ($\alpha<0.1$). Over-curing, which is properly predicted with the processing chart, has a direct impact on thermo-mechanical properties and causes the thermal oxidation of the resin resulting in a significant loss of the glass transition temperature. Thermal oxidation darkens the resin.

CRediT authorship contribution statement

S. Zaidi: Writing – review & editing, Investigation, Formal analysis. **S. Thakur:** Writing – review & editing, Investigation. **D. Sanchez-Rodriguez:** Writing – original draft, Investigation, Formal analysis, Conceptualization. **R. Verdejo:** Writing – review & editing, Resources. **J. Farjas:** Writing – review & editing, Supervision. **J. Costa:** Writing – review & editing, Supervision, Project administration, Funding acquisition.

Declaration of competing interest

The authors declare that they have no known competing financial interests or personal relationships that could have appeared to influence the work reported in this paper.

Data availability

Data will be made available on request.

Acknowledgements

The authors acknowledge AMADE and the GRMT project (PID2021–126989OB-I00 financed by the MCI, Spain). We also thank the Catalan Government for their support through 2017SGR1378. D.S.R. acknowledges the support received from the Beatriu de Pinós Programme and the Ministry of Research and Universities of the Government of Catalonia (Fellowship BP00069). S.T. acknowledges the SABIO project (PID2020–119546RJ-I00) financed by the MCIN/AEI, Spain.

Supplementary materials

Supplementary material associated with this article can be found, in the online version, at doi:10.1016/j.polymdegradstab.2024.110743.

References

[1] F.L. Jin, X. Li, S.J. Park, Synthesis and application of epoxy resins: a review, J. Ind. Eng. Chem. 29 (2015) 1–11, https://doi.org/10.1016/j.jiec.2015.03.026.
[2] R. Hsissou, R. Seghiri, Z. Benzekri, M. Hilali, M. Rafik, A. Elharfi, Polymer composite materials: a comprehensive review, Compos. Struct. 262 (2021) 0–3, https://doi.org/10.1016/j.compstruct.2021.113640.
[3] S. Liu, V.S. Chevali, Z. Xu, D. Hui, H. Wang, A review of extending performance of epoxy resins using carbon nanomaterials, Compos. Part B Eng. 136 (2018) 197–214, https://doi.org/10.1016/j.compositesb.2017.08.020.
[4] O.R.Z. Fuhhs, D.Q.G.E. Fduhixo, I. Jrrg, S. Dw, H. Whpshudwxuhv, W. Zlwkrxw, V. Lpsdlulqj, W. Rwkhu, G. Hqjlqhhulqj, Z. Yhu, K. Lpsdfw, U. Lv, U. Iru, W.K.H. Erqghg, T oughening Epoxy Adhesives to Meet Today ' s Challenges, (2003) 445–448.
[5] Z. Ahmadi, Nanostructured epoxy adhesives: a review, Prog. Org. Coatings. 135 (2019) 449–453, https://doi.org/10.1016/j.porgcoat.2019.06.028.
[6] L.K. Aggarwal, P.C. Thapliyal, S.R. Karade, Anticorrosive properties of the epoxy-cardanol resin based paints, Prog. Org. Coatings. 59 (2007) 76–80, https://doi.org/10.1016/j.porgcoat.2007.01.010.
[7] V.C. Malshe, G. Waghoo, Weathering study of epoxy paints, Prog. Org. Coatings. 51 (2004) 267–272, https://doi.org/10.1016/j.porgcoat.2004.07.007.
[8] K. Kowalczyk, T. Spychaj, Epoxy coatings with modified montmorillonites, Prog. Org. Coatings. 62 (2008) 425–429, https://doi.org/10.1016/j.porgcoat.2008.03.001.
[9] M.M.A. Baig, M.A. Samad, Epoxy\epoxy composite\epoxy hybrid composite coatings for tribological applications—a review, Polymers (Basel) 13 (2021) 1–27, https://doi.org/10.3390/polym13020179.
[10] J. Liu, L. Zhang, W. Shun, J. Dai, Y. Peng, X. Liu, Recent development on bio-based thermosetting resins, J. Polym. Sci. 59 (2021) 1474–1490, https://doi.org/10.1002/pol.20210328.
[11] M. Samper, J. Ferri, A. Carbonell, R. Balart, O. Gimeno, Properties of biobased epoxy resins from epoxidized linseed oil (ELO) crosslinked with a mixture of cyclic anhydride and maleinized linseed oil, Express Polym. Lett. 13 (2019) 407–418, https://doi.org/10.3144/expresspolymlett.2019.34.
[12] Q. Fu, J. Tan, C. Han, X. Zhang, B. Fu, F. Wang, X. Zhu, Synthesis and curing properties of castor oil-based triglycidyl ether epoxy resin, Polym. Adv. Technol. 31 (2020) 2552–2560, https://doi.org/10.1002/pat.4982.
[13] S. Hirose, T. Hatakeyama, H. Hatakeyama, Novel epoxy resins derived from biomass components, Procedia Chem. 4 (2012) 26–33, https://doi.org/10.1016/j.proche.2012.06.004.
[14] J.T. Miao, L. Yuan, Q. Guan, G. Liang, A. Gu, Biobased heat resistant epoxy resin with extremely high biomass content from 2,5-furandicarboxylic acid and eugenol, ACS Sustain. Chem. Eng. 5 (2017) 7003–7011, https://doi.org/10.1021/acssuschemeng.7b01222.
[15] E. Savonnet, E. Grau, S. Grelier, B. Defoort, H. Cramail, Divanillin-based epoxy precursors as DGEBA substitutes for biobased epoxy thermosets, ACS Sustain. Chem. Eng. 6 (2018) 11008–11017, https://doi.org/10.1021/acssuschemeng.8b02419.
[16] E.K. Pye, Industrial lignin production and applications, biorefineries-industrial process, Prod. Status Quo Futur. Dir. 2 (2008) 165–200, https://doi.org/10.1002/9783527619849.CH22.
[17] M. Fache, B. Boutevin, S. Caillol, Vanillin, a key-intermediate of biobased polymers, Eur. Polym. J. 68 (2015) 488–502, https://doi.org/10.1016/j.eurpolymj.2015.03.050.
[18] M.B. Hocking, Vanillin: synthetic flavoring from spent sulfite liquor, J. Chem. Educ. 74 (1997) 1055–1059, https://doi.org/10.1021/ed074p1055.
[19] M. Machado, M. Hofmann, M. Garrido, J.R. Correia, J.C. Bordado, I.C. Rosa, Incorporation of lignin in bio-based resins for potential application in fiber–polymer composites, Appl. Sci. 13 (2023), https://doi.org/10.3390/app13148342.
[20] E. Desnoes, L. Toubal, A.H. Bouazza, D. Montplaisir, Biosourced vanillin Schiff base platform monomers as substitutes for DGEBA in thermoset epoxy, Polym. Eng. Sci. 60 (2020) 2593–2605, https://doi.org/10.1002/pen.25497.
[21] M. Zhi, X. Yang, R. Fan, S. Yue, L. Zheng, Q. Liu, Y. He, Sustainable vanillin-based epoxy resin with excellent flame retardancy and mechanical properties, ACS Appl. Polym. Mater. 5 (2023) 1312–1324, https://doi.org/10.1021/acsapm.2c01863.
[22] L.C. Chan, H.N. Naé, J.K. Gillham, Time-temperature–transformation (TTT) diagrams of high Tg epoxy systems: competition between cure and thermal degradation, J. Appl. Polym. Sci. 29 (1984) 3307–3327, https://doi.org/10.1002/app.1984.070291109.
[23] Q. Li, X. Li, Y. Meng, Curing of DGEBA epoxy using a phenol-terminated hyperbranched curing agent: cure kinetics, gelation, and the TTT cure diagram, Thermochim. Acta. 549 (2012) 69–80, https://doi.org/10.1016/j.tca.2012.09.012.
[24] J.B. Enns, J.K. Gillham, P.M. Program, Time-temperature-transformation (TTT) cure diagram : modeling the cure behavior of thermosets below Tgm, J. Appl. Polym. Sci. 28 (1983) 2567–2591.
[25] C.K. Tziamtzi, K. Chrissafis, Optimization of a commercial epoxy curing cycle via DSC data kinetics modelling and TTT plot construction, Polymer (Guildf) 230 (2021), https://doi.org/10.1016/j.polymer.2021.124091.
[26] D. Sanchez-Rodriguez, S. Zaidi, Y. Jahani, A. Ruiz de Luzuriaga, A. Rekondo, P. Maimi, J. Farjas, J. Costa, Processability and reprocessability maps for vitrimers considering thermal degradation and thermal gradients, Polym. Degrad. Stab. 217 (2023) 110543, https://doi.org/10.1016/j.polymdegradstab.2023.110543.
[27] F. González Garcia, B.G. Soares, V.J.R.R. Pita, R. Sánchez, J. Rieumont, Mechanical properties of epoxy networks based on DGEBA and aliphatic amines, J. Appl. Polym. Sci. 106 (2007) 2047–2055, https://doi.org/10.1002/app.24895.
[28] J. Galy, A. Sabra, J.-P. Pascault, Characterization of epoxy thermosetting systems by differential scanning calorimetry, Polym. Eng. & Sci. 26 (1986) 1514–1523, https://doi.org/10.1002/pen.760262108.
[29] M. Javdanitehran, D.C. Berg, E. Duemichen, G. Ziegmann, An iterative approach for isothermal curing kinetics modelling of an epoxy resin system, Thermochim. Acta. 623 (2016) 72–79, https://doi.org/10.1016/j.tca.2015.11.014.
[30] N. Sbirrazzuoli, S. Vyazovkin, A. Mititelu, C. Sladic, L. Vincent, A study of epoxy-amine cure kinetics by combining isoconversional analysis with temperature modulated DSC and dynamic rheometry, Macromol. Chem. Phys. 204 (2003) 1815–1821, https://doi.org/10.1002/macp.200350051.
[31] D. Sánchez-Rodríguez, H. Eloussifi, J. Farjas, P. Roura, M. Dammak, Thermal gradients in thermal analysis experiments: criterions to prevent inaccuracies when determining sample temperature and kinetic parameters, Thermochim. Acta. 589 (2014), https://doi.org/10.1016/j.tca.2014.05.001.

[32] J. Coates, Interpretation of Infrared Spectra, A Practical Approach, Encycl. Anal. Chem. (2000) 10815–10837, https://doi.org/10.1002/9780470027318.a5606.
[33] S. Vyazovkin, N. Sbirrazzuoli, Mechanism and kinetics of epoxy-amine cure studied by differential scanning calorimetry, Macromolecules 29 (1996) 1867–1873, https://doi.org/10.1021/ma951162w.
[34] S. Vyazovkin, D. Dollimore, Linear and nonlinear procedures in isoconversional computations of the activation energy of nonisothermal reactions in solids, J. Chem. Inf. Comput. Sci. 36 (1996) 42–45, https://doi.org/10.1021/ci950062m.
[35] H.L. Friedman, Kinetics of thermal degradation of char-forming plastics from thermogravimetry. Application to a phenolic plastic, J. Polym. Sci. Part C Polym. Symp. 6 (1964) 183–195, https://doi.org/10.1002/polc.5070060121.
[36] L. Luo, X. Guo, Z. Zhang, M. Chai, M.M. Rahman, X. Zhang, J. Cai, Insight into pyrolysis kinetics of lignocellulosic biomass: isoconversional kinetic analysis by the modified friedman method, Energy and Fuels 34 (2020) 4874–4881, https://doi.org/10.1021/acs.energyfuels.0c00275.
[37] S. Vyazovkin, P.K.B.T.-H. of T.A., Chapter 13 - Isoconversional Kinetics, in: M. E. Brown, C. Gallagher (Eds.), Recent Adv. Tech. Appl., Elsevier Science B.V., 2008, pp. 503–538, https://doi.org/10.1016/S1573-4374(08)80016-7.
[38] J. Farjas, P. Roura, Isoconversional analysis of solid-state transformations: a critical review. Part III. Isothermal and non isothermal predictions, J. Therm. Anal. Calorim. 109 (2012) 183–191, https://doi.org/10.1007/s10973-011-1642-2.
[39] S. Rasi, P. Roura-Grabulosa, J. Farjas, Application of thermal analysis and kinetic predictions to YBCO films prepared by chemical solution deposition methods, J. Therm. Anal. Calorim. 142 (2020) 2077–2086, https://doi.org/10.1007/s10973-020-10103-4.
[40] D.A. Frank-Kamenetskii, Diffusion and Heat Exchange in Chemical Kinetics, 2nd ed., Princeton University Press, New Jersey, 1955.
[41] A.G. Merzhanov, A.E. Averson, The present state of the thermal ignition theory: an invited review, Combust. Flame. 16 (1971) 89–124, https://doi.org/10.1016/S0010-2180(71)80015-9.
[42] D. Sánchez-Rodriguez, J. Farjas, P. Roura, The critical condition for thermal explosion in an isoperibolic system, AIChE J 63 (2017), https://doi.org/10.1002/aic.15727.
[43] L. Sorrentino, L. Tersigni, A method for cure process design of thick composite components manufactured by closed die technology, Appl. Compos. Mater. 19 (2012) 31–45, https://doi.org/10.1007/s10443-010-9179-2.
[44] L. Esposito, L. Sorrentino, F. Penta, C. Bellini, Effect of curing overheating on interlaminar shear strength and its modelling in thick FRP laminates, Int. J. Adv. Manuf. Technol. 87 (2016) 2213–2220, https://doi.org/10.1007/s00170-016-8613-5.
[45] I. Fraga, S. Montserrat, J.M. Hutchinson, Vitrification and devitrification during the non-isothermal cure of a thermoset. Theoretical model and comparison with calorimetric experiments, Macromol. Chem. Phys. 211 (2010) 57–65, https://doi.org/10.1002/macp.200900322.
[46] D. Santiago, X. Fernández-Francos, X. Ramis, J.M. Salla, M. Sangermano, Comparative curing kinetics and thermal-mechanical properties of DGEBA thermosets cured with a hyperbranched poly(ethyleneimine) and an aliphatic triamine, Thermochim. Acta. 526 (2011) 9–21, https://doi.org/10.1016/j.tca.2011.08.016.
[47] D. Santín, O. Konuray, X. Fernàndez-Francos, X. Ramis, Kinetics analysis and simulation of sequential epoxy dual-curing systems with independent thermal activation, Thermochim. Acta. 673 (2019) 158–168, https://doi.org/10.1016/j.tca.2019.01.023.
[48] N. Areny, O. Konuray, X. Fernàndez-Francos, J.M. Salla, J.M. Morancho, X. Ramis, Time-temperature-transformation (TTT) diagram of a dual-curable off-stoichiometric epoxy-amine system with latent reactivity, Thermochim. Acta. 666 (2018) 124–134, https://doi.org/10.1016/j.tca.2018.06.012.
[49] S. Vyazovkin, N. Sbirrazzuoli, Isoconversional kinetic analysis of thermally stimulated processes in polymers, Macromol. Rapid Commun. 27 (2006) 1515–1532, https://doi.org/10.1002/marc.200600404.
[50] F. Chambon, H.H. Winter, Linear Viscoelasticity at the Gel Point of a Crosslinking PDMS with Imbalanced Stoichiometry, J. Rheol. (N. Y. N. Y) 31 (1987) 683–697, https://doi.org/10.1122/1.549955.
[51] W. Brostow, S.H. Goodman, J. Wahrmund, 8 - Epoxies, in: H. Dodiuk, S.H.B.T.-H. of T.P. (Third E. Goodman (Eds.), William Andrew Publishing, Boston, 2014: pp. 191–252. https://doi.org/10.1016/B978-1-4557-3107-7.00008-7.
[52] Z. Zhu, X. Sun, H. Yuan, C. Song, Y. Cao, X. Li, Determination of gel time and gel point of epoxy-amine thermosets by in-situ near infrared spectroscopy, Polym. Test. 72 (2018) 416–422, https://doi.org/10.1016/j.polymertesting.2018.11.001.
[53] Paul J. Flory Jr., Principles of Polymer Chemistry, Cornell University Press, 1954.
[54] A.T. DiBenedetto, Prediction of the glass transition temperature of polymers: a model based on the principle of corresponding states, J. Polym. Sci. Part B Polym. Phys. 25 (1987) 1949–1969, https://doi.org/10.1002/polb.1987.090250914.
[55] J.P. Pascault, R.J.J. Williams, Relationships between glass transition temperature and conversion - Analyses of limiting cases, Polym. Bull. 24 (1990) 115–121, https://doi.org/10.1007/BF00298330.
[56] R. Delannoy, V. Tognetti, E. Richaud, Structure–Properties Relationships Involved in the Embrittlement of Epoxies, Polymers (Basel) 14 (2022), https://doi.org/10.3390/polym14214685.
[57] P.S. Sindhu, N. Mitra, D. Ghindani, S.S. Prabhu, Epoxy Resin (DGEBA/TETA) exposed to water: a spectroscopic investigation to determine water-epoxy interactions, J. Infrared, Millimeter, Terahertz Waves. 42 (2021) 558–571, https://doi.org/10.1007/s10762-021-00788-5.
[58] E. Ernault, E. Richaud, B. Fayolle, Thermal oxidation of epoxies: influence of diamine hardener, Polym. Degrad. Stab. 134 (2016) 76–86, https://doi.org/10.1016/j.polymdegradstab.2016.09.030.
[59] F. Rothenhäusler, H. Ruckdaeschel, Interplay of curing and thermal degradation in epoxy resins cured with amino acids: influence of the maximum curing temperature on the network structure, crystal morphology and mechanical properties, J. Appl. Polym. Sci. (2023) 1–15, https://doi.org/10.1002/app.54655.
[60] Y. Zahra, F. Djouani, B. Fayolle, M. Kuntz, J. Verdu, Thermo-oxidative aging of epoxy coating systems, Prog. Org. Coatings. 77 (2014) 380–387, https://doi.org/10.1016/j.porgcoat.2013.10.011.
[61] J. Ma, G. Li, X. Hua, N. Liu, Z. Liu, F. Zhang, L. Yu, X. Chen, L. Shang, Y. Ao, Biodegradable epoxy resin from vanillin with excellent flame-retardant and outstanding mechanical properties, Polym. Degrad. Stab. 201 (2022) 109989, https://doi.org/10.1016/j.polymdegradstab.2022.109989.
[62] M.I. Martín, F. Rodríguez-Lence, A. Güemes, A. Fernández-López, L.A. Pérez-Maqueda, A. Perejón, On the determination of thermal degradation effects and detection techniques for thermoplastic composites obtained by automatic lamination, Compos. Part A Appl. Sci. Manuf. 111 (2018) 23–32, https://doi.org/10.1016/j.compositesa.2018.05.006.
[63] J. Mangialetto, R. Verhelle, G. Van Assche, N. Van Den Brande, B. Van Mele, Time-Temperature-Transformation, Temperature-Conversion-Transformation, and Continuous-Heating-Transformation Diagrams of Reversible Covalent Polymer Networks, Macromolecules 54 (2021) 412–425, https://doi.org/10.1021/acs.macromol.0c02491.
[64] J.E.K. Schawe, A description of chemical and diffusion control in isothermal kinetics of cure kinetics, Thermochim. Acta. 388 (2002) 299–312, https://doi.org/10.1016/S0040-6031(02)00041-2.
[65] S.A. Schwartz, R.A. Bubeck, Physical aging in thermosets of differing degrees of cure—Master curve generation and the relation to mechanical properties, Polym. Eng. Sci. 28 (1988) 1–5, https://doi.org/10.1002/pen.760280102.
[66] J.C. Arnold, The influence of physical aging on the creep rupture behavior of polystyrene, J. Polym. Sci. Part B Polym. Phys. 31 (1993) 1451–1458, https://doi.org/10.1002/polb.1993.090311102.
[67] M. Song, Modulated differential scanning calorimetry observation of physical ageing in polymers, J. Therm. Anal. Calorim. 63 (2001) 699–707, https://doi.org/10.1023/A:1010131802572.
[68] S. Montserrat, Y. Calventus, J.M. Hutchinson, Physical aging of thermosetting powder coatings, Prog. Org. Coatings. 55 (2006) 35–42, https://doi.org/10.1016/j.porgcoat.2005.10.005.
[69] T. Instruments, Measurement of Glass Transition Temperatures by Dynamic Mechanical Analysis and Rheology, Meas. Glas. Transit. Temp. by Dyn. Mech. Anal. Rheol. (2000) 1–5.
[70] T.E. Twardowski, S.E. Lin, P.H. Geil, Curing in Thick Composite Laminates: experiment and Simulation, J. Compos. Mater. 27 (1993) 216–250, https://doi.org/10.1177/002199839302700301.
[71] P.R. Ciriscioli, Q. Wang, G.S. Springer, Autoclave Curing — Comparisons of Model and Test Results, J. Compos. Mater. 26 (1992) 90–102, https://doi.org/10.1177/002199839202600106.
[72] T.A. Bogetti, J.W. Gillespie, Two-Dimensional Cure Simulation of Thick Thermosetting Composites, J. Compos. Mater. 25 (1991) 239–273, https://doi.org/10.1177/002199839102500302.
[73] Curing : it ' s a Matter of Time (t), Temperature (T) and Pressure (P), (n.d.). https://doi.org/10.1016/B978-1-85617-415-2.50007-1.